APPLICATIONS OF SONOCHEMISTRY TO MATERIALS SYNTHESIS

K.S. SUSLICK, M.M. FANG, T. HYEON, M.M. MDLELENI
Department of Chemistry
University of Illinois at Urbana-Champaign
601 S. Goodwin Ave., Urbana, IL 61801, USA

1.   Introduction

One of the most important recent applications of sonochemistry has been to the synthesis and modification of inorganic materials [1-5]. In liquids irradiated with high intensity ultrasound, acoustic cavitation drives bubble collapse producing intense local heating, high pressures, and very short lifetimes; these transient, localized hot spots drive high energy chemical reactions [5-11]. As described in detail elsewhere in this monograph, these hot spots have temperatures of roughly 5000°C, pressures of about 1000 atmospheres, and heating and cooling rates above 10^{10} K/s. Thus, cavitation serves as a means of concentrating the diffuse energy of sound into a unique set of conditions to produce unusual materials from dissolved (and generally volatile) solution precursors.

Ultrasonic cavitation in liquid-solid systems produces related phenomena. Cavity collapse near an extended solid surface becomes non-spherical, drives high-speed jets of liquid into the surface, and creates shockwave damage to the surface [11]. This process can produce newly exposed, highly heated surfaces and is responsible for the erosion/corrosion problems associated with hydrodynamic cavitation [12]. Furthermore, during ultrasonic irradiation of liquid-powder slurries, cavitation and the shockwaves it creates can accelerate solid particles to high velocities [13, 14]. As discussed later, the interparticle collisions that result are capable of inducing striking changes in surface morphology, composition, and reactivity [1-5, 14].

There is a wide range of chemical and physical consequences that high intensity can induce, as shown schematically in Figure 1. The chemical effects of ultrasound fall into three areas: homogeneous sonochemistry of liquids, heterogeneous sonochemistry of liquid-liquid or liquid-solid systems, and sonocatalysis (which overlaps the first two). Applications of ultrasound to materials chemistry are found in all of these areas. Chemical reactions are not generally seen in the ultrasonic irradiation of solids or solid-gas systems.

To demonstrate the utility of sonochemistry in materials synthesis, we will examine a range of applications discovered at the University of Illinois. Specifically,

we will describe the sonochemical synthesis and heterogeneous catalytic studies of nanostructured amorphous iron and alloys, nanostructured Fe on silica, nanocolloids of Fe, and nanostructured Mo_2C and MoS_2. In addition, we will summarize earlier studies on the effects of high intensity ultrasound on slurries of inorganic solids.
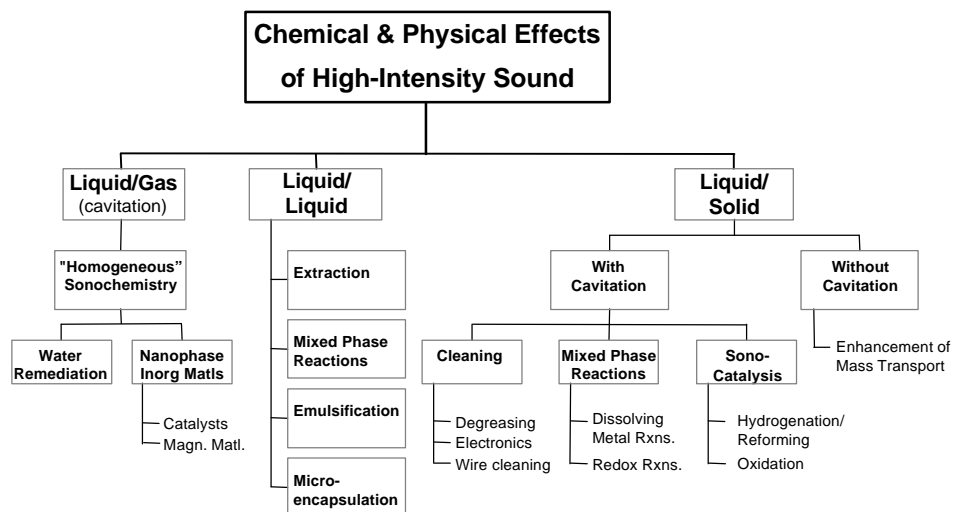
Figure 1. Classification of the chemical and physical effects of ultrasound.

2.   Synthesis of Nanostructured Inorganic Materials

Solids made from nanometer sized components often exhibit properties distinct from those of the bulk, in part because clusters that small have electronic structures that have a high density of states, but not yet continuous bands [15-17]. Such nanostructured materials have been a matter of intense current interest, and several preparative methods have been developed for their synthesis. Nanostructured material syntheses include both gas phase techniques (e.g., molten metal evaporation, flash vacuum thermal and laser pyrolysis decomposition of volatile organometallics), liquid phase methods (e.g., reduction of metal halides with various strong reductants, colloid techniques with controlled nucleation), and mixed phase approaches (e.g., synthesis of conventional heterogeneous catalysts on oxide supports, metal atom vapor deposition into cryogenic liquids, explosive shock synthesis). To this range of techniques, over the past ten years we have added the sonochemical reactions of volatile organometallics as a general approach to the synthesis of nanophase materials, as shown in Figure 2.
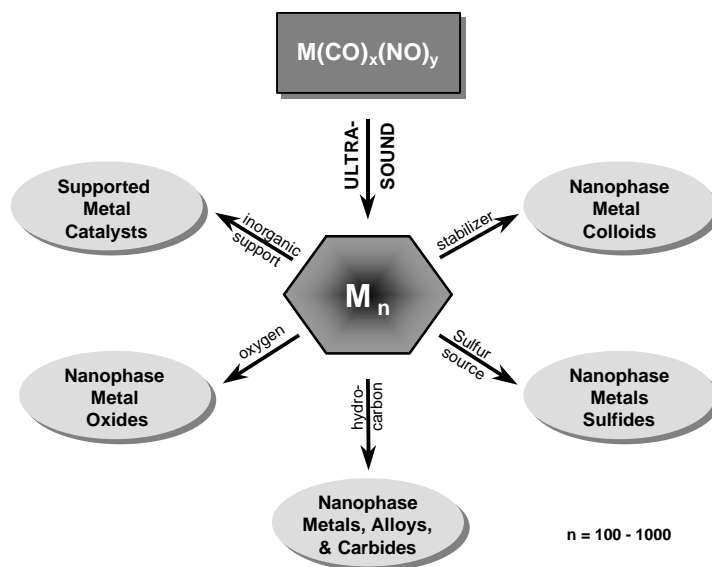
Figure 2. Sonochemical synthesis of nanostructured materials.

Using these extreme conditions, we have produced a variety of nanostructured and often amorphous metals, alloys, and carbides and examined their catalytic activity [1-4, 18-33]. Volatile organometallic compounds decompose inside a collapsing bubble, and the resulting metal atoms agglomerate to form nanostructured materials. Our sonochemical synthesis of nanostructured materials is also extremely versatile: various forms of nanophase materials can be generated simply by changing the reaction medium (Figure 2). When precursors are sonicated in high boiling alkanes, nanostructured metal powders are formed. If sonication occurs in the presence of a bulky or polymeric surface ligand, stable nanophase metal colloids are created. Sonication of the precursor in the presence of an inorganic support (silica or alumina) provides an alternative means of trapping the nanometer clusters. These nanoparticles trapped upon these supports produce active supported heterogeneous catalysts.

2.1.   EXPERIMENTAL CONSIDERATIONS

High-intensity ultrasonic probes [50 to 500 W/cm^2] of the type used for biological cell disruption are the most reliable and effective source for laboratory-scale sonochemistry. A typical apparatus that permits easy control over ambient temperature and atmosphere is shown in Fig. 3. Lower acoustic intensities can often be used in liquid-solid heterogeneous systems, because of the reduced liquid tensile strength at

the liquid-solid interface. For such reactions, a common ultrasonic cleaning bath will therefore often suffice. The low intensity available in these devices [$\approx$ 1 W/cm^2], however, can prove limiting. In addition, the standing wave patterns in ultrasonic cleaners require accurate positioning of the reaction vessel. On the other hand, ultrasonic cleaning baths are easily accessible, relatively inexpensive, and useable on moderately large scale. Finally, for larger scale irradiations, flow reactors with high ultrasonic intensities are commercially available in modular units of as much as 20 kW [34, 35].
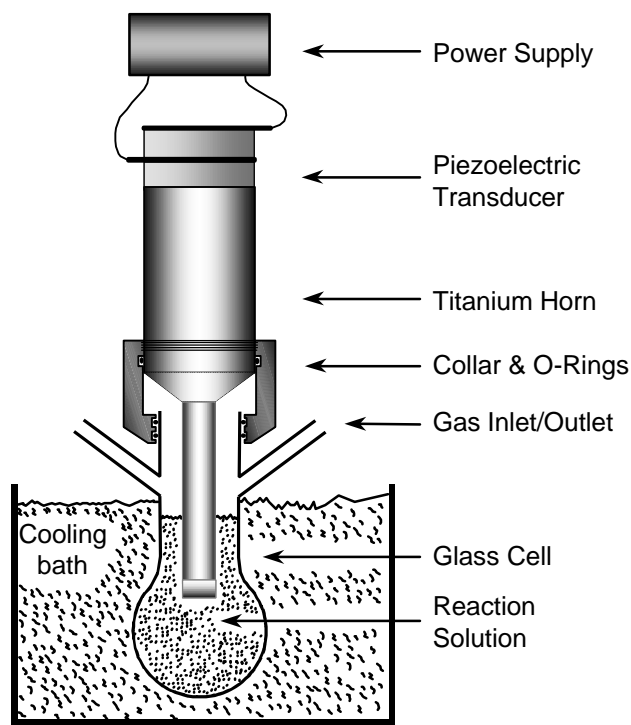
Figure 3. A typical sonochemical apparatus with direct immersion ultrasonic horn. Ultrasound can be easily introduced into a chemical reaction with good control of temperature and ambient atmosphere. The usual piezoelectric ceramic is PZT, a lead zirconate titanate ceramic. Similar designs for sealed stainless steel cells can operate at pressures above 10 bar.

Sonochemical decomposition rates for volatile organometallic compounds depend on a variety of experimental parameters such as vapor pressure of precursors, solvent vapor pressure, and ambient gas. In order to achieve high sonochemical yields, the precursors should be highly volatile since the primary sonochemical reaction site is the vapor inside the cavitating bubbles [36]. So that decomposition takes place only during cavitation, thermal stability is also important. In addition, the solvent vapor

pressure should be low at the sonication temperature, because significant solvent vapor inside the bubble reduces the bubble collapse efficiency.

2.2.   AMORPHOUS METALS

The ultrasonic irradiation of solutions containing volatile transition metal carbonyls (e.g., $Fe(CO)_5$, $Ni(CO)_4$, $Co(CO)_3NO$) produces highly porous aggregates of nanometer-sized clusters of amorphous metals [18-21]. For example, sonication of 1 M iron pentacarbonyl in decane at 0 ^{o}C under argon flowing yielded a dull black powder. Elemental analysis of the powder, after heating at 100 ^{o}C under vacuum to remove residual solvent, showed it to be >96 % iron by weight, with trace amounts of carbon (<3%) and oxygen (1%, by difference), presumably from the decomposition of alkane solvent or carbon monoxide during ultrasonic irradiation. Scanning electron micrographs (SEM) revealed that the powder is an agglomerate of 20 nm particles (Figure 4). Transmission electron micrographs (TEM) further indicated that these 20 nm particles consist of smaller 4~6 nm particles.

Figure 4. Amorphous iron prepared by the sonochemical decomposition of $Fe(CO)_5$ [18].

The amorphous nature of the iron powder was confirmed by several different techniques, including SEM, differential scanning calorimetry (DSC), electron microdiffraction, X-ray powder diffraction, and neutron diffraction. Initial X-ray powder diffraction showed no diffraction peak; after heat treatment under helium at

350 ^{o}C the diffraction lines characteristic of bcc iron metal are observed. Electron microdiffraction revealed a diffuse ring pattern, characteristic of amorphous materials. DSC also shows one exothermic irreversible disorder-order transition temperature at 308 ^{o}C. The amorphous metal formation appears to result from the extremely high cooling rate during acoustic cavitation.

There had been a long-standing controversy concerning the magnetic properties of amorphous iron, which had not been previously available without substantial amount of added alloying elements (e.g., boron). Magnetic studies of the sonochemically prepared amorphous iron showed that amorphous iron is a very soft ferromagnetic with a saturation magnetization of ≈173 EMU/g and a Curie temperature in excess of 580K. The effective magnetic moment is 1.7 μ_B with an effective exchange constant of only ≈30% of crystalline Fe [20]. The neutron diffraction data [21] confirmed these measurements and was consistent with a random packing model, as in many thin amorphous metal films. The magnetic properties fall close to those of liquid iron.

2.3.   NANOSTRUCTURED ALLOYS

Sonochemical techniques can also be used to prepare nanostructured alloys. We chose Fe/Co alloys as a demonstration case because $Fe(CO)_5$ and $Co(CO)_3(NO)$ were readily available as precursors that are thermally stable at the modest bulk solution temperatures necessary for high volatility. The composition of the Fe-Co alloys can be controlled simply by changing the ratio of solution concentrations of the precursors; alloy compositions ranging from pure Fe to pure Co are readily obtained [23-25].
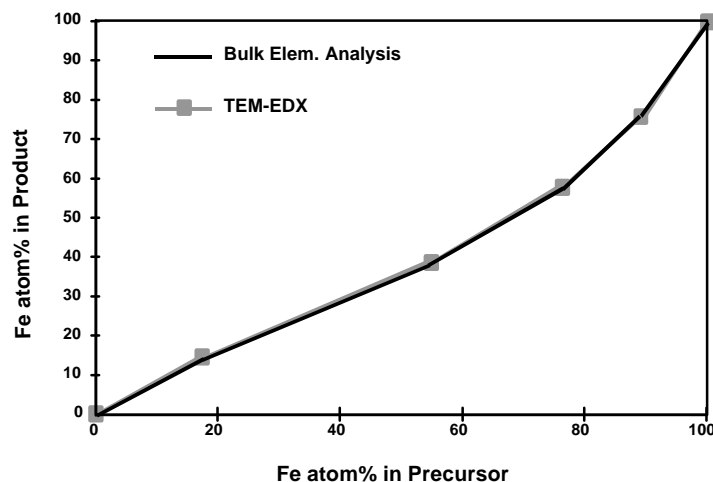
Figure 5. Bulk and nanometer Energy Dispersive X-ray (EDX) analysis of Fe/Co alloys prepared sonochemically from $Fe(CO)_5$ and $Co(CO)_3NO$ [23].

The solid-solution nature of the alloys was confirmed by Energy Dispersive X-ray (EDX) measurements. Analyses made on various nanometer spots showed that the alloys were homogeneous on a nanometer scale and were consistent with bulk elemental analysis (Figure 5). The Fe, Co, and Fe-Co alloys produced by ultrasound are initially amorphous, as determined by XRD and electron-beam microdiffraction. After heat treatment under H_2 gas flow at 400°C for 2 hours, all samples underwent crystallization. The XRD results show no peaks attributable to iron/cobalt oxide, iron/cobalt carbide or other iron/cobalt impurity phases. Pure Fe crystallizes to cubic (bcc) structure, and pure Co crystallizes to cubic (fcc) and hexagonal (hcp) mixed structures. All the alloys that we have tested so far crystallize in the bcc structure. This result is consistent with the known Fe-Co equilibrium phase diagram that strongly favors the bcc structure. Elemental analysis results show that nearly pure metal and alloys are produced after H_2 treatment. SEM at high magnification indicates that these materials are porous aggregates of small clusters of 10-20 nm particles. Surface electronic structures and surface compositions of the sonochemically prepared Fe-Co alloys were also examined by using x-ray photoelectron spectroscopy (XPS). The XPS measurements have been performed on heat-treated samples before catalytic reactions. The electronic structures of the surfaces of these samples appear to be the same as the pure metals. The surface compositions of the alloys demonstrate a slight enrichment of Fe over Co. Similar trends towards an iron-enriched surface have been reported by other researchers with other preparations using coprecipitation methods [37].

Heterogeneous catalysts containing two metals often show unusual activity or selectivity for a wide range of industrially important reactions [38-40]. For this reason, we made catalytic studies of the sonochemically prepared Fe-Co alloys for hydrocarbon dehydrogenation and hydrogenolysis reactions. In general, dehydrogenation of hydrocarbons is the important and desirable reaction, and hydrogenolysis (to methane generally) is a wasteful side-reaction. Unfortunately, most metals (with the notable exception of Pt and other noble metals) are much too active as hydrogenolysis catalysts to be commercially useful. The suppression of hydrocarbon cracking during dehydrogenation remains an important challenge for non-platinum catalysts.

All catalysts were treated under H_2 gas flow at 400°C for 2 hours before the catalytic studies. While this does not alter the size of the clusters that make up the nanostructure of these materials significantly, it does cause their crystallization. H_2 treatment is necessary, however, to provide a reproducible catalytic surface. Two kinds of products were formed during the cyclohexane reaction: benzene from the dehydrogenation reaction and aliphatic hydrocarbons (mostly methane) from the hydrogenolysis. The catalytic selectivity (in terms of the percentage of benzene among all the reaction products) as a function of temperature is shown in Figure 6.

The catalytic properties of the sonochemically prepared Fe, Co and Fe-Co alloys in the cyclohexane reaction exhibit interesting trends. First, they are all active catalysts for cyclohexane conversion: pure Co has the highest activity (albeit primarily for hydrogenolysis), pure Fe has the lowest activity, and Fe-Co alloys are intermediate. Second, Fe-Co alloys generate much more dehydrogenation product (benzene) than pure Fe or Co. Third, the 1:1 Fe/Co alloy has both much higher dehydrogenation

activities and selectivities at all reaction temperatures (250°C to 300°C) than the other alloys or pure metals. In the best cases, the selectivity for dehydrogenation approaches 100%. We believe that the increase in selectivity comes from a selective poisoning of the sites responsible for hydrogenolysis. Fe/Co alloys prepared conventionally with very high purity do *not* show high selectivity for dehydrogenation *unless* they are pre-treated with methane or carbon monoxide at high temperatures in order to deposit a small amount of surface carbon. The sonochemical preparations inevitably produce catalysts with small amounts of surface carbon and hence with high dehydrogenation selectivity.
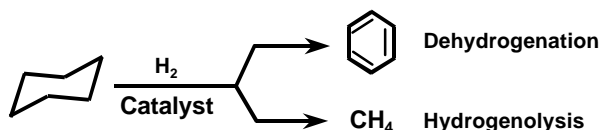
	Hydrogenolysis	Dehydrogenation
Product	**Methane**	**Benzene**
Surface structure	**Sensitive**	**Insensitive**
Active site	**Ensemble of metal atoms**	**Single metal atoms**
Active catalyst	**Ru, Os, most metals**	**Pt**

Figure 6. Catalytic dehydrogenation versus hydrogenolysis.
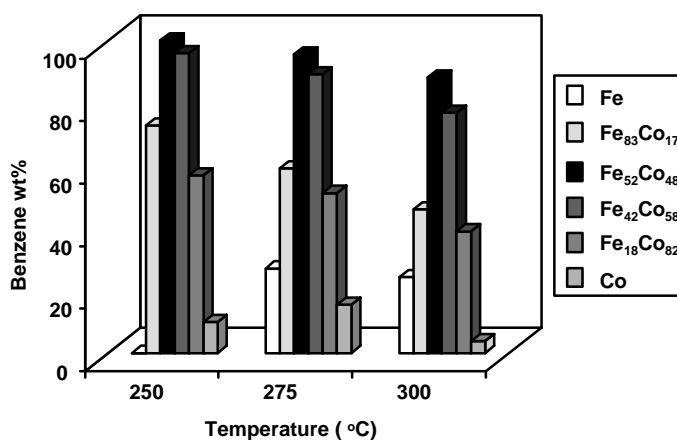
Figure 7. Selectivity for cyclohexane dehydrogenation (to benzene) over hydrogenolysis (to methane) by sonochemically prepared Fe/Co alloys [23].

2.4.   NANOSTRUCTURED SUPPORTED "EGGSHELL" CATALYSTS

Most heterogeneous metal catalysts are supported, i.e., the metal is deposited on a high surface area solid, such as silica or alumina. In general, these materials are made by taking simple metal salts (usually the nitrates), soaking aqueous solutions of them into the porous support, and calcining under hydrogen at high temperatures to produce small metal particles throughout the support. Often, the metal particles are not very uniform and are dispersed throughout the ill-defined pore structure of the support. The creation of "eggshell" catalysts where uniform-sized nanoparticles of metals are deposited on the outer surface of supports has potential advantages for catalyst preparation [40].

Ultrasonic irradiation of decane solutions of iron pentacarbonyl, $Fe(CO)_5$, in the presence of silica gel produces a silica-supported amorphous nanostructured iron in which the iron particles are all on the outer surface of the silica [23, 28]. The iron particles are formed during cavitation events and then deposited on the silica suspended in solution. The iron loading on the SiO_2 can be easily varied by changing the initial concentration of the $Fe(CO)_5$ solution. Elemental analysis reveals Fe, Si, O and a trace amount of carbon (<1%) to be present.

The amorphous nature of these supported iron particles as initially deposited has been confirmed by several different techniques, including DSC, XRD, and electron-beam microdiffraction. DSC shows one irreversible exothermic transition at 335°C corresponding to a disorder-order transition (i.e., crystallization) of the amorphous iron. X-ray powder diffraction shows no diffraction peaks from the initial products. After heat treatment under He at 400°C for 4 hours (sufficient to induce crystallization), the lines characteristic of α-Fe metal are observed, and no peaks can be attributed to iron oxide, iron carbide or other iron-based phases. Electron microdiffraction by transmission electron microscopy (TEM) confirms these observations.

The TEM showed that the iron particles produced by sonolysis of $Fe(CO)_5$ were highly dispersed on the SiO_2 surface. The iron particles range in size from 3 to 8 nm; CO chemisorption measurement data at -78°C on our samples gives an average iron particle size of 7 nm. The particles are on the surface of the silica only, which gives a very different surface morphology to the silica compared to a conventionally prepared catalyst (Figure 8).

The catalytic activity of the silica supported nanostructured iron was probed in the commercially important Fischer-Tropsch synthesis reaction (i.e., hydrogenation of CO). Under our conditions, the major reaction products for both catalysts are short-chain C_1 to C_4 hydrocarbons and CO_2. The catalytic activity of the sonochemically produced iron on silica catalyst is an order of magnitude higher than the conventional supported iron at similar loadings and dispersions. Moreover, the silica-supported nanostructured iron catalyst exhibits high activity at low temperatures (<250°C), where the conventional catalyst has no activity. The dramatic difference in activity between the two samples below 300°C may be due to the amorphous nature of iron and the inherently highly-defected surface formed during sonolysis of $Fe(CO)_5$ when the

amorphous state of iron is preserved. At higher temperatures, the activity decreases, which may be due to iron crystallization, surface annealing, or catalyst deactivation from surface carbon deposition.

Conventionally Prepared Catalyst

Sonochemically Prepared "Eggshell" Catalyst

Figure 8. Scanning electron micrographs of conventionally and sonochemically prepared

iron catalysts supported on silica.

2.5.   NANOCOLLOIDS

The existence of aggregates of nanometer clusters in our sonochemically prepared materials suggests the possibility of trapping these particles before they aggregate. Colloids of ferromagnetic materials are of special interest due to their many important technological applications as ferrofluids [41, 42]. Such magnetic fluids find uses in information storage media, magnetic refrigeration, audio reproduction, and magnetic sealing. Commercial magnetic fluids are generally produced by exhaustive grinding of magnetite (Fe_3O_4) in ball or vibratory mills for several weeks in the presence of surfactants, which produces a very broad particle size distribution [41, 42]. We have developed a new method for the preparation of stable ferromagnetic colloids of iron using high intensity ultrasound to sonochemically decompose volatile organometallic compounds [31]. These colloids have narrow size distributions centered at a few nanometers and are found superparamagnetic.

Sonochemical decomposition of iron pentacarbonyl in the presence of stabilizers such as polyvinylpyrrolidone or oleic acid produced a colloid of nanometer sized iron particles [31]. Transmission electron micrographs show that the iron particles have a relatively narrow range in size from 3 to 8 nm for polyvinylpyrrolidone, while oleic acid gives an even more uniform distribution at 8 nm (Figure 9). Electron microdiffraction revealed that the particles are amorphous on the nanometer scale as formed and that after *in situ* electron beam heating these particles crystallize to bcc iron.
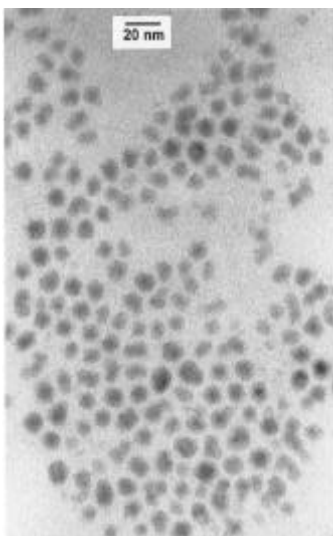
Figure 9. Transmission electron micrograph of sonochemically-prepared
iron colloid stabilized by oleic acid [31].

Magnetic studies indicate that these colloidal iron particles are superparamagnetic with a saturation magnetization of a respectable 101 emu/g (Fe) at 290K. High saturation magnetization is desirable for magnetic fluid application and is highly sensitive to the method of preparation. Bulk amorphous Fe saturates at 156 emu/g (Fe) [20, 21, 30]. For a comparison, the saturation magnetization of a commercial magnetite-based magnetic fluid is 123 emu/g (Fe) (Ferrofluids Corp., Cat. #APG-047)

2.6.   NANOSTRUCTURED MOLYBDENUM CARBIDE

Molybdenum and tungsten carbides have been explored as heterogeneous catalysts because of the similarity in activity that these carbides share with platinum group metals [43-45]. For catalytic applications, high surface-area materials are generally needed, but the refractory nature of these carbides makes this very difficult. Boudart and Volpe prepared carbides of molybdenum and tungsten with high surface areas by a complex temperature programmed carburization of the corresponding nitrides. We have developed a simple sonochemical synthesis of nanophase molybdenum carbide from the ultrasonic irradiation of molybdenum hexacarbonyl [25-29].

Sonochemical decomposition of molybdenum hexacarbonyl in hexadecane produced a black powder. After heat treatment at 450°C under He flow for 12 hours, peaks in the XRD were observed at d spacing values of 2.39 Å, 1.49 Å, and 1.27 Å, which match very well with face centered cubic (fcc) molybdenum carbide, Mo_2C. The formation of molybdenum carbide can be explained by the disproportionation of carbon monoxide on the active metal surface to form carbon and carbon dioxide. Small amounts of residual oxygen were removed by treating the solid with 1:1 CH_4/H_2 mixture at 300 to 500 °C for 48 h. The elemental analysis results showed that the sample had a stoichiometry of $Mo_2C_{1.02}$ with less than 0.09 wt. % oxygen (by difference) and <0.02 wt. % hydrogen. The XRD was essentially unchanged by carburization. SEM showed that the surface is extremely porous. TEM revealed that the material is a porous aggregate of 3 nm diameter particles (Figure 10); BET gas adsorption showed a surface area of 130 m^2/g.

Again, the dehydrogenation versus hydrogenolysis of cyclohexane served as our standard reaction using a flow catalytic microreactor. To compare the catalytic properties, commercial ultrafine powders of platinum and ruthenium (Aldrich Chemicals Co., 0.27 - 0.47 μm diameter) were also used under identical conditions, after heating at 400ºC for 3 h under H_2 flow to remove surface contaminants. Figure 11 shows the catalytic activity as a function of temperature for the Mo_2C sample pretreated under CH_4/H_2 at 500 ºC for 48 hours compared to commercial ultrafine Pt powder.

At all reaction temperatures examined, benzene was the only product formed for both samples and their activities were comparable: no hydrogenolysis products were detected. In contrast, only hydrogenolysis, mostly to methane, occurred with commercial ruthenium powder. The analogy has often been made that Mo_2C is similar to Ru whereas W_2C behaves like Pt [46]. These results demonstrate, however, that for

dehydrogenation of alkanes, sonochemically prepared nanostructured molybdenum carbide has selectivity similar to Pt rather than to Ru.

Figure 10. TEM and electron microdiffraction of sonochemically prepared Mo_2C.
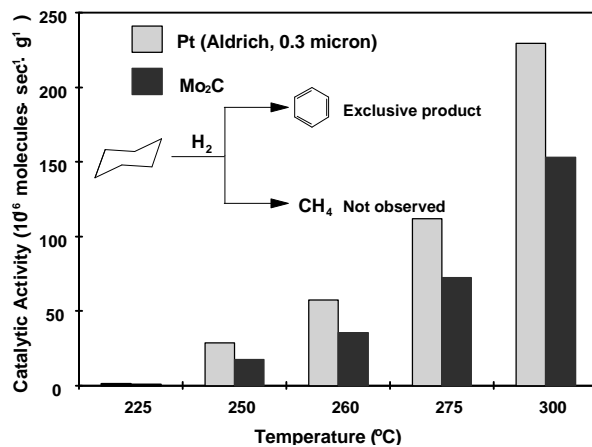
Figure 11. Catalytic activity of sonochemically prepared Mo_2C compared to Pt [27].

2.7. NANOSTRUCTURED MOLYBDENUM SULFIDE

Very recently, we have reported the sonochemical synthesis of nanostructured molybdenum sulfide. MoS_2 is best known as the standard automotive lubricant; its lubricant properties are due to its layered structure. Planes of molybdenum atoms are sandwiched on both faces by planes of sulfur atoms tightly bonded to the Mo. Interactions between the sulfur planes are weak, thus producing lubrication properties similar to graphite. Of greater interest here, however, MoS_2 is also the predominant hydrodesulfurization catalyst heavily used by the petroleum industry to remove sulfur from fossil fuels before combustion [39].

We prepared an unusual morphology of MoS_2 by the irradiation of solutions of molybdenum hexacarbonyl and sulfur in 1,2,3,5-tetramethylbenzene with high intensity ultrasound [33]. The MoS_2 was amorphous as initially prepared, but subsequently crystallized upon heating at $450^{\circ}C$ for 10 h under an atmosphere of flowing He. EDX analysis performed on these particles gave a S/Mo atomic ratio of 2.06, identical within experimental error to bulk chemical analysis. The morphologies of the sonochemical and conventional MoS_2, however, are dramatically different, as shown in Figure 12. Conventional MoS_2 shows a plate-like morphology typical for such layered materials. The sonochemical MoS_2 exists as a porous agglomeration of clusters of spherical particles with an average diameter of 15 nm.

Despite the morphological difference between the sonochemical and conventional MoS_2, TEM images (Figure 13) of these sulfides both show lattice fringes with interlayer spacings of 0.62 ± 0.01 nm, the same as conventional MoS_2 [47]. The sonochemically prepared MoS_2, however, shows much greater edge and defect content, as the layers must bend, break or otherwise distort to fit outer surface of the 15 nm particle size (Fig. 13).

It is well established that the activity of MoS_2 is localized at the edges and not on the flat basal planes [39, 48]. Unfortunately, the nature of this layered material causes the basal planes to dominate the total surface area under most synthetic conditions. Given the inherently higher edge concentrations in nanostructured materials, the catalytic properties of our sonochemically prepared MoS_2 become especially interesting. To this end, the catalytic activity and selectivity for thiophene HDS by sonochemically prepared MoS_2 was examined in a single-pass microreactor [33]. Conventional MoS_2, sonochemical Mo_2C, commercial ReS_2 (Gallard-Schlesinger Ind., Carle Place, NY), and RuS_2 (Gallard-Schlesinger) were also investigated under the same conditions for comparison. For conventionally prepared sulfides, ReS_2 and RuS_2 are inherently more reactive than MoS_2 [48], but are too expensive to be generally used. Given the difference in edge versus basal surface activity, catalytic activity does not correlate with total surface area and therefore comparisons must be made on a catalyst mass basis.

Conventional MoS$_2$

Sonochemical MoS$_2$

Figure 12. Morphology of conventional and sonochemically prepared MoS$_2$ [33].

Figure 13. TEM of sonochemically prepared MoS_2. Basal planes are seen as dark fringes
with interlayer spacings of 0.62 ± 0.01 nm, the same as conventional MoS_2 [33].

The observed turnover frequencies as a function of temperature for these catalysts are shown in Figure 14. The principal products detected by GC were the C_4 hydrocarbons: butadiene, 1-butene, *trans*-2-butene, *cis*-2-butene, and butane. No partially hydrogenated thiophenes were detected, and lighter (C_1-C_3) hydrocarbons accounted for less than 1% of the reaction products. The observed HDS activity order is MoS_2 (sonochemical) > RuS_2 (conventional) > ReS_2 (conventional) ~ Mo_2C (sonochemical[11]) > MoS_2 (conventional). The sonochemically prepared MoS_2 catalyzes the hydrodesulfurization (HDS) of thiophene with activities roughly five-fold better than conventional MoS_2 and comparable to those observed with RuS_2, one of the best commercial catalysts.
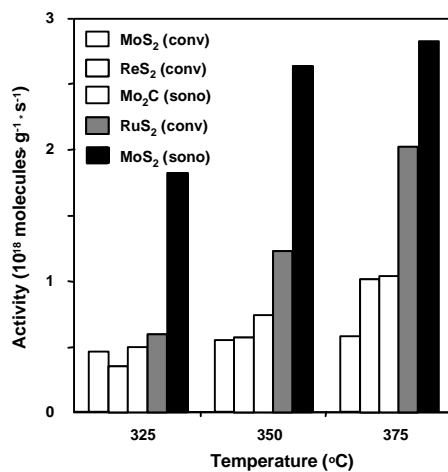
Figure 14. Catalytic activity for hydrodesulfurization of thiophene by various catalysts [33].

The product selectivities, expressed as percent of total C_4 hydrocarbons, observed at 375 ^{o}C were also examined. All the catalyst studied show high selectivity for butenes with the exception of the sonochemical MoS_2, which is selective to butane. The accepted mechanism for thiophene HDS involves initial hydrogenolysis of the C-S bonds to give butadiene, followed by rapid hydrogenation to 1-butene, which is subsequently hydrogenated to butane or isomerized to a thermodynamic mixture of *cis-* and *trans-*2-butenes [39]. It is not surprising to see increased butane production from the sonochemical MoS_2, given its higher HDS activity.

There remains much to explore in the sonochemical synthesis of inorganic materials, and this technique has only begun to be exploited. The use of ultrasound in the synthesis of metal oxides, for example, has some promise as well [49-50].

3.   Sonochemical Synthesis Of Biomaterials

Another important application of sonochemistry to materials chemistry has been the preparation of biomaterials, most notably protein microspheres [51-57]. While the chemical effect of ultrasound on aqueous solutions have been studied for many years, the development of aqueous sonochemistry for biomaterials synthesis is very recent, particularly in the area of microencapsulation. It is beyond the scope of this chapter to review this area thoroughly, but a brief synopsis and bibliography will be provided.

Using high intensity ultrasound and simple protein solutions, a remarkably easy method to make both air-filled microbubbles and nonaqueous liquid-filled microcapsules has been developed. Figure 15 shows an electron micrograph of sonochemically prepared microspheres. These microspheres are stable for months, and being slightly smaller than erythrocytes, can be intravenously injected to pass unimpeded through the circulatory system.

Figure 15. Scanning electron micrograph of sonochemically prepared

protein microspheres from bovine serum albumin [6].

The mechanism responsible for microsphere formation is a combination of *two* acoustic phenomena: emulsification and cavitation. Ultrasonic emulsification creates the microscopic dispersion of the protein solution necessary to form the proteinaceous microspheres. Alone, however, emulsification is insufficient to produce long-lived microspheres. The long life of these microspheres comes from a sonochemical cross-linking of the protein shell. Chemical reactions requiring O_2 are critical in forming the microspheres. It has been known for some time that the primary products from the sonolysis of water are H_2 and H_2O_2 coming from the sonolysis of water yielding $H^.$ and $OH^.$; in the presence of O_2, the latter produces HO_2 [58]. Based on chemical trapping experiments, we established that the proteinaceous microspheres are held together by disulfide bonds between protein cysteine residues and that superoxide is the crosslinking agent, as shown schematically in Figure 16. The crosslinked shell of the microspheres is only about ten protein molecules thick, as shown in Figure 17.
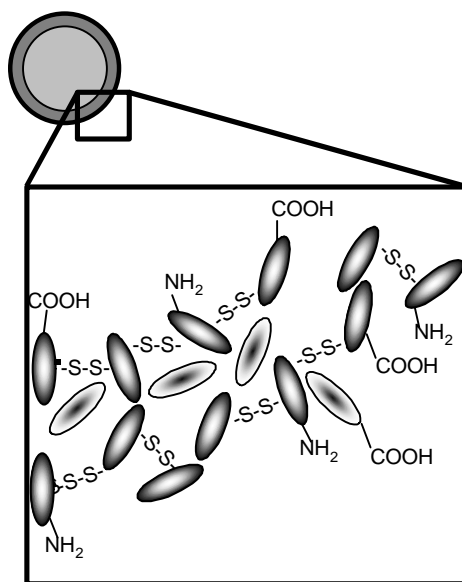
Figure 16. Schematic of the disulfide crosslinking that holds the protein microspheres together.

These protein microspheres, have a wide range of biomedical applications, including their use as echo contrast agents for sonography [59], magnetic resonance imaging contrast enhancement [54, 56, 57], oxygen or drug delivery [55], among others. An extensive patent literature now exists in this area [60-71].
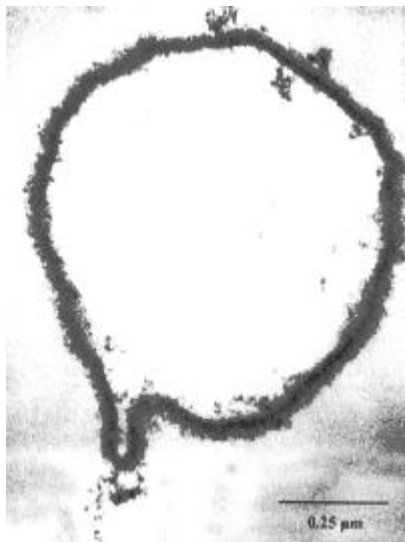
Figure 17. Transmission electron micrograph of protein-stained microtome section
from a sonochemically prepared protein microspheres [55].

4.   Sonochemical Modification of Inorganic Materials

The use of ultrasound to accelerate chemical reactions in liquid-solid heterogeneous systems has become increasingly widespread. The sonochemical enhancement the reactivity of reactive metals as stoichiometric reagents has become an especially routine synthetic technique for many heterogeneous organic and organometallic reactions [4, 6, 9-10, 72-75], particularly those involving reactive metals, such as Mg, Li or Zn. Rate enhancements of more than tenfold are common, yields are often substantially improved, and byproducts avoided. This development originated from the early work of Renaud and the more recent breakthroughs of Luche. The effects are quite general and apply to reactive inorganic salts and to main group reagents as well. Less work has been done with unreactive metals (e.g., Ni, V, Nb, Mo, W), but results here are promising as well [76, 77].

The physical phenomena primarily responsible for such enhancements include improvement of mass transport from turbulent mixing and acoustic streaming, the generation of surface damage at liquid-solid interfaces by shock waves and microjets, the generation of high-velocity interparticle collisions in slurries, and the fragmentation of friable solids to increase surface area. We will focus our attention here on the last three of these.

In examining heterogeneous sonochemistry for either stoichiometric and catalytic reactions, one must adopt techniques not often employed by synthetic

chemists. It is important to use both chemical kinetic and surface characterization techniques. The following protocol has proved quite successful in such investigations: (1) monitor the kinetics of the chemical reactivity of the solids, both during sonication and following irradiation of the solid in the absence of substrate, (2) determine effects of irradiation on surface morphology and size distributions of powders and solids by electron microscopy, and (3) measure surface composition depth profiles and composition by Auger electron spectroscopy (AES), EDX, and XPS. The power of this three-pronged approach has been proved in studies of the sonochemistry of transition metal powders [14, 76-80].

4.1.   SURFACE CAVITATION

Cavitation near extended liquid-solid interfaces is very different from cavitation in pure liquids [11, 12]. There are general physical mechanisms responsible for the effects of cavitation near surfaces: microjet impact and shockwave damage. Whenever a cavitation bubble is produced near a boundary, the asymmetry of the liquid particle motion during cavity collapse often induces a deformation in the cavity (as shown schematically in Figure 18. The potential energy of the expanded bubble is converted into kinetic energy of a liquid jet that extends through the bubble's interior and penetrates the opposite bubble wall. Because most of the available energy is transferred to the accelerating jet, rather than the bubble wall itself, this jet can reach velocities of hundreds of meters per second. Because of the induced asymmetry, the jet often impacts the local boundary and can deposit enormous energy densities at the site of impact. Such energy concentration can result in severe damage to the boundary surface.

Figure 18. Formation of a liquid microjet during bubble collapse near an extended surface.

The second mechanism of cavitation-induced surface damage invokes shockwaves created by cavity collapse in the liquid [11]. The impingement of microjets and shockwaves on the surface creates the localized erosion responsible for ultrasonic cleaning and many of the sonochemical effects on heterogeneous reactions. The erosion of metals by cavitation can generate newly exposed, highly heated surfaces and even eject metal from the surface. The importance of this process to corrosion and erosion phenomena of metals and machinery has been thoroughly reviewed elsewhere [12].

4.2.   INTERPARTICLE COLLISIONS

Distortions of bubble collapse depend on a surface several times larger than the resonance bubble size. Thus, for ultrasonic frequencies of ≈20 kHz, damage associated with microjet formation cannot occur for solid particles smaller than ≈200 μm. This takes on a special importance for sonochemistry, since fine powders are generally preferred for use as solid reagents or catalysts.

In liquid-solid slurries, cavitation still occurs, however, and the bubble collapse will still launch shock waves out into the liquid. When these shock waves pass over particles in close proximity to one another, high-velocity interparticle collisions can result. If the collision is at a direct angle, metal particles can be driven together at sufficiently high speeds to induce effective melting at the point of collision [13, 14], as seen in Figures 19 and 20. From the volume of the melted region of impact, the amount of energy generated during collision was determined. From this, a lower estimate of the velocity of impact was several hundred m/s, or roughly one half the speed of sound!

Before ultrasound   15 min. ultrasound   120 min. ultrasound
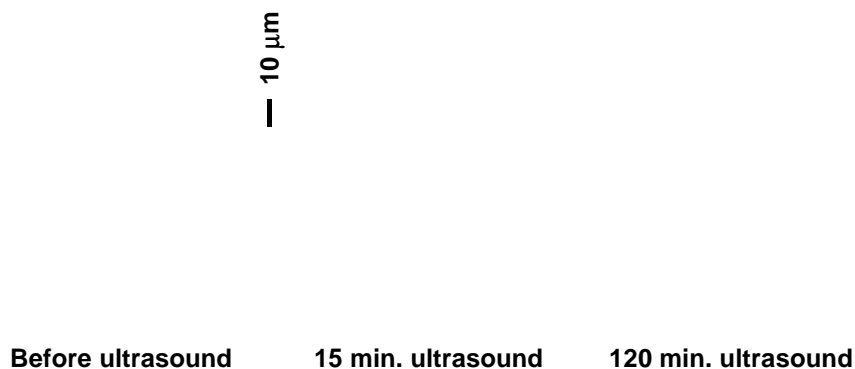
Figure 19. The effect of ultrasonic irradiation on aggregation of Ni powder as a slurry in decane [76].

Figure 20. Scanning electron micrograph of Zn powder
after ultrasonic irradiation as a slurry in decane [13].

Before ultrasound   **60 min. ultrasound**

Figure 21. The effect of ultrasonic irradiation on the surface morphology of Ni powder. High-velocity
interparticle collisions caused by ultrasonic irradiation of slurries is responsible for these effects [80].

If the particles collide at a glancing angle, a mechanical removal of surface material results with a macroscopic smoothing (and at the atomic level, a microscopic roughening) of the surface (as shown in Figure 21), in analogy to lapidary ball milling. Especially for reactive metals that form oxide, nitride or carbonaceous coatings, the consequences to the reactivity of metal particles can be quite substantial [3, 4, 14, 76-80]. Surface composition studies with depth profiling by Auger electron spectroscopy and by sputtered neutral mass spectrometry reveal that ultrasonic irradiation effectively removes surface oxide and other contaminating coatings [14, 76-80]. An example of such an analysis is shown in Figure 22. The removal of such passivating coatings can dramatically improve chemical reaction rates. The reactivity of clean metal surfaces also appears to be responsible for the greater tendency for heterogeneous sonochemical reactions to involve single electron transfer [81] rather than acid-base chemistry, which generally arises from surface sites of the oxide coatings.
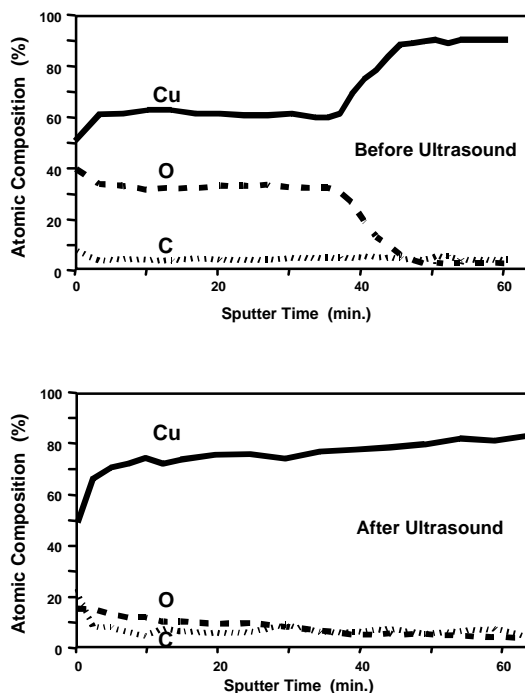
Figure 22. The effect of ultrasonic irradiation of Cu powder slurries on the surface composition.
50 min. sputter time is roughly 1 μm depth [78].

In order to probe the conditions created during interparticle collisions in slurries irradiated with ultrasound, a series of transition metal powders were examined (Figure 23). Using the irradiation of Cr, Mo, and W powders in decane at 20 kHz and 50 W/cm^2, one observes agglomeration and what appears to be localized melting for the first two metals, but not the third [13]; the melting points of these metals are 1857° for Cr, 2617° for Mo, and 3410°C for W. If one compiles a table of the effects of ultrasonic irradiation of slurries of different metal powders (Figure 24), one discovers that there is a break point in aggregation and surface deformations that occurs as the metal melting points increase. It appears that the effective transient temperature reached at the point of impact during interparticle collisions is roughly 3000°C. This effective local temperature has no direct connection with the temperatures inside the cavitating bubble, but they are another demonstration of the extreme conditions which ultrasound can create in an otherwise cold liquid.

Before ultrasound **30 min. ultrasound**
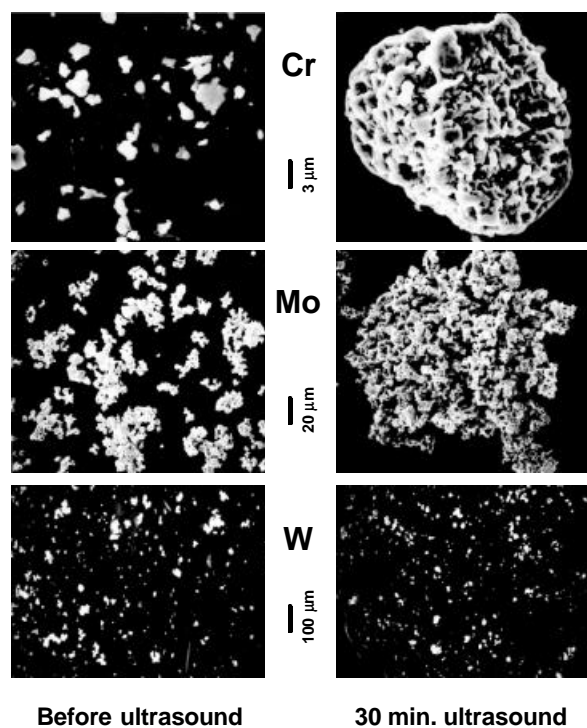
Figure 23. Scanning electron micrograph of Cr, Mo, and W powder after ultrasonic irradiation of decane slurries under Ar. The melting points of these metals are 1857°, 2617°, and 3410°C, respectively [13].

METAL	MELTING POINT	AGGLOME-RATION	SURFACE MORPHOLOGY
Sn	505 K	++	++
Zn	693 K	++	++
Cu	1358 K	++	++
Ni	1726 K	++	++
Cr	2130 K	++	+
Mo	2890 K	+	-
W	3680 K	-	-

20 kHz, 50 W/cm^2, 293 K, 10 μm powder, in decane under Ar.

Figure 24. The effects of ultrasonic irradiation on slurries of metal powders [14].

For brittle solids, interparticle collisions can also induce fragmentation. This can substantially increase the available surface area of the powders and thus enhance liquid-solid reaction rates. An example of this effect is found in the application of ultrasound to the process of molecular intercalation into layered inorganic solids [82, 83]. The adsorption of organic or inorganic compounds between the atomic sheets of layered solids permits the systematic change of optical, electronic, and catalytic properties. Such materials have many technological applications (for example, lithium batteries, hydrodesulfurization catalysts, and solid lubricants). The kinetics of intercalation, however, are generally extremely slow, and syntheses usually require high temperatures and very long reaction times. High-intensity ultrasound dramatically increases the rates of intercalation (by as much as 200-fold) of a wide range of compounds (including amines, metallocenes, and metal sulfur clusters) into various layered inorganic solids (such as ZrS_2, V_2O_5, TaS_2, MoS_2, and MoO_3). SEM of the layered solids coupled to chemical kinetics studies demonstrated that the origin of the observed rate enhancements comes from particle fragmentation (which dramatically increases surface areas), and to a lesser extent from surface damage. The activation of heterogeneous reagents, especially non-metals, often arises from this effect. The effects of ultrasound on silica, for example, can substantially alter reactivity patterns [75].

4.3.   EFFECTS OF ULTRASOUND ON HETEROGENEOUS CATALYSIS

Catalytic reactions are of enormous importance in both laboratory and industrial applications. Heterogeneous catalysts often require rare and expensive metals. The use of ultrasound offers some hope of activating less reactive, but also less costly, metals. Such effects can occur in three distinct stages: (1) during the formation

of supported catalysts, (2) activation of preformed catalysts, or (3) enhancement of catalytic behavior during a catalytic reaction. Some early investigations of the effects of ultrasound on heterogeneous catalysis can be found in the Soviet literature [3, 84]. In this early work, increases in turnover rates were usually observed upon ultrasonic irradiation, but were rarely more than tenfold. In the cases of modest rate increases, it appears likely that the cause is increased effective surface area; this is especially important in the case of catalysts supported on brittle solids (e.g., noble metals supported on carbon).

More impressive effects, however, have been reported [3], especially for hydrogenations and hydrosilations with Ni or Raney Ni powder. For example, as shown in Figure 25, the hydrogenation of alkenes by Ni powder is enormously enhanced by ultrasonic irradiation [76, 80]. This is not due to fragmentation of the solid: the surface area did not change significantly even after lengthy irradiation. There is, however, a very interesting effect on the surface morphology (Figures 19 and 21). Ultrasonic irradiation smoothes, at a macroscopic scale, the initially crystalline surface and causes agglomeration of small particles. Both effects are due to interparticle collisions caused by cavitation-induced shockwaves. AES revealed that there is a striking decrease in the thickness of the oxide coat after ultrasonic irradiation. It is the removal of this passivating layer that is responsible for the $>10^5$-fold increase observed in catalytic activity.
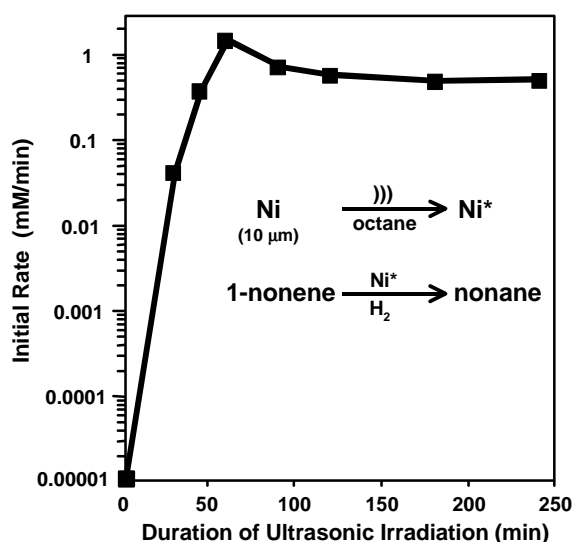
Figure 25. Effect of ultrasonic irradiation of Ni slurries in octane
on its activity as a hydrogenation catalyst [3].

5.   Conclusion

A diverse set of applications of ultrasound to enhancing chemical reactivity has been explored, with important applications in mixed phase synthesis, materials chemistry, and biomedical uses. Bubble collapse in liquids results in an enormous concentration of energy from the conversion of the kinetic energy of liquid motion into heating of the contents of the bubble. The enormous local temperatures and pressures so created provide a unique means for fundamental studies of chemistry and physics under extreme conditions. For example, the sonochemical decomposition of volatile organometallic precursors in high boiling solvents produces nanostructured materials in various forms with high catalytic activities. Nanostructured metals, alloys, carbides and sulfides, nanometer colloids, and nanostructured supported catalysts can all be prepared by this general route. Cavitation can also have dramatic effects on the reactivities of both extended solid surfaces and on fine powders. Microjet and shock wave impact (on large surfaces) and interparticle collisions (with powders) have substantial effects on the chemical composition and physical morphology of solids that can dramatically enhance chemical reactivity.

6.   Acknowledgments

7.   References

1.   Suslick, K.S. (1995) *MRS Bulletin 20*, 29.
2.   Suslick, K.S. (1993) Ultrasound: Applications to Materials Chemistry, in *Encyclopedia of Materials Science and Engineering*; Cahn, R.W., ed.; Pergamon Press, Oxford; 3rd Suppl., pp. 2093-2098.
3.   Suslick, K.S. (1997) Sonocatalysis, in *Handbook of Heterogeneous Catalysis*; Ertl, G.; Knozinger, H.; Weitkamp, J.; eds.; Wiley-VCH, Weinheim; vol. 3, ch. 8.6, pp. 1350-57.
4.   Suslick, K.S. (1994) Sonochemistry of Transition Metal Compounds, in *Encyclopedia of Inorganic Chemistry*; King, R.B., ed.; J. Wiley & Sons, New York, vol. 7, pp. 3890-3905.
5.   Suslick, K.S.; Crum, L.A. (1997) Sonochemistry and Sonoluminescence, in *Encyclopedia of Acoustics*; Crocker, M.J., ed.; Wiley-Interscience, New York, vol. 1, ch. 26, pp. 271-282.
6.   Suslick, K.S. (1998) Sonochemistry, in *Kirk-Othmer Encyclopedia of Chemical Technology*; 4th Ed. J. Wiley & Sons, New York, vol. 26, 517-541.
7.   Flint, E.B.; Suslick, K.S. (1991) *Science* **253**, 1397.
8.   Suslick, K.S. (1990) *Science*, **247**, 1439.
9.   Suslick, K.S., ed. (1988) *Ultrasound: Its Chemical, Physical, and Biological Effects*, VCH Publishers, New York.
10.   Mason, T.J., Lorimer, J.P. (1988) *Sonochemistry: Theory, Applications and Uses of Ultrasound in Chemistry,* Ellis Horword, Ltd., Chichester, U.K.
11.   Leighton, T.G. (1994) *The Acoustic Bubble* Academic Press, London, pp. 531-551.
12.   Preece, C.M., Hansson, I.L. 1981 *Adv. Mech. Phys. Surf.* **1**, 199.
13.   Doktycz, S.J., Suslick, K.S. (1990) *Science* **247**, 1067.
14.   Suslick, K.S., Doktycz, S.J. (1990) The Effects of Ultrasound on Solids in *Advances in Sonochemistry*, Mason, T.J., ed., JAI Press, New York, pp. 197-230.
15.   Weller, H. (1993) *Adv. Mater.* **5**, 88.
16.   Moser, W.R., ed. (1996) *Advanced Catalysts and Nanostructured Materials;* Academic Press: New York.
17.   Gleiter, H. (1992) *Adv. Mater.* **4**, 474.
18.   K.S. Suslick, S.B. Choe, A.A. Cichowlas, M.W. Grinstaff (1991) *Nature* **353**, 414.
19.   Grinstaff, M.W.; Cichowlas, A.A.; Choe, S.B.; Suslick, K.S., (1992) *Ultrasonics* **30**, 168.
20.   Grinstaff, M.W.; Salamon, M.B.; Suslick, K.S. (1993) *Phys. Rev. B* **48**, 269.
21.   Bellissent, R.; Galli, G.; Grinstaff, M.W.; Migliardo, P.; Suslick, K.S. (1993) *Phys. Rev. B* **48**, 15797-15800.
22.   Suslick, K.S.; Hyeon, T.; Fang, M.; Cichowlas, A.A. (1994) *Molecularly Designed Nanostructured Materials*, MRS Symp. Proc., v. 351. Gonsalves, K.E.; Chow, G.M.; Xiao, T.O.; Cammarata, R.C., eds. Materials Research Society, Pittsburgh,, pp. 201-206.
23.   Suslick, K.S.; Fang, M.; Hyeon, T.; Cichowlas, A.A. (1994) *Molecularly Designed Nanostructured Materials*, MRS Symp. Proc., v. 351. Gonsalves, K.E.; Chow, G.M.; Xiao, T.O.; Cammarata, R.C., eds. Materials Research Society, Pittsburgh, pp. 443-448.
24.   Bellissent, R.; Galli, G.; Hyeon, T.; Magazu, S.; Majolino, D.; Migliardo, P.; Suslick, K.S. (1995) *Phys. Scripta* **T57**, 79-83.
25.   Hyeon, T.; Fang, M.; Cichowlas, A.A.; Suslick, K.S. (1995) *Matl. Sci. Eng. A,* **204**, 186-192.
26.   Suslick, K.S.; Hyeon, T.; Fang, M.; Ries, J.T.; Cichowlas, A.A. (1996) *Materials Science Forum* (Transtec Publ., N.Y.), **225-227***,* 903-912 .
27.   Hyeon, T.; Fang, M.; Suslick, K.S. (1996) *J. Am. Chem. Soc.* **118**, 5492-5493.
28.   Suslick, K.S.; Hyeon, T.; Fang, M; Cichowlas, A.A. (1996) Sonochemical Preparation of Nanostructured Catalysts, *Advanced Catalysts and Nanostructured Materials;* Moser, W.R., ed. Academic Press, New York, pp. 197-211.
29.   Suslick, K.S.; Hyeon, T.; Fang, M. (1996) *Chem. Materials* **8,** 2172-2179.
30.   Bellissent, R.; Galli, G.; Hyeon, T.; Migliardo, P.; Parette, P.; Suslick, K.S. (1996) *J. Noncryst. Solids*, **205-207**, 656-659.
31.   Suslick, K.S.; Fang, M.; Hyeon, T. (1996) *J. Am. Chem. Soc.*, **118**, 11960-11961.
32.   Long, G.J.; Hautot, D.; Pankhurst, Q.A.; Vandormael, D.; Grandjean, F.; Gaspard, J.P.; Briois V.; Hyeon. T.; Suslick, K.S. (1998) *Phys. Rev. B*, in press.
33.   Mdleleni, M.M.; Hyeon, T.; Suslick, K.S. (1998) *J. Am. Chem. Soc.*, **120***,* 6189-90.
34.   Hunicke, R.L. (1990) *Ultrasonics* **28**, 291.
35.   Mason, T.J.; Cordemans, E.D. (1996) *Chem. Eng. Res. Des.* **74**, 511.

36. Suslick, K.S.; Cline, Jr., R.E.; Hammerton, D. A. (1986) *J. Amer. Chem. Soc.* **106**, 5641.
37. Nishizawa, T.; Ishida, K. (1984) *Bull. Alloy Phase Diagrams* **5**, 250.
38. Sinfelt, J.H. (1983) *Bimetallic Catalysts: Discoveries, Concepts, and Applications,* J. Wiley & Sons, New York, pp. 18-31.
39. Gates, B.C. (1992) *Catalytic Chemistry*; John Wiley & Sons, New York; pp. 387-392.
40. Klabunde, K.J.; Li, Y.-X. (1993)*Selectivity in Catalysis*; Davis, M.E., Suib, S.L., Eds.; American Chemical Society, Washington, D.C., pp. 88-108 and references therein.
41. Fertman, V.E. (1990) *Magnetic Fluids Guidebook: Properties and Applications*; Hemisphere Publishing Co., New York.
42. Berkovsky, B.M.; Medvedev, V.F.; Krakov, M.S. (1993) *Magnetic Fluids: Engineering Applications*; Oxford University Press, Oxford.
43. Ranhotra, G.S.; Haddix, G.W.; Bell, A.T.; Reimer, J.A. (1987) *J. Catal.* **108**, 40.
44. Lee, J.S.; Oyama, S.T.; Boudart, M. (1990) *J. Catal.*, **125**, 157.
45. Ledoux, M.J.; Pham-Huu, C.; Guille, J.; Dunlop, H. (1992) *J. Catal.* **134**, 383.
46. Volpe, L.; Boudart, M. (1985) *J. Solid State Chem.* **59**, 332.
47. Inamura, K.; Prins, R. (1994) *J. Catal.* **147**, 515.
48. Pecoraro, T.A.; Chianelli, R.R. (1981) *J. Catal.* **67**, 430.
49. Cao, X.; Prozorov, R.; Koltypin, Y; Kataby, G; Felner, I.; Gedanken, A. (1997) *J. Mater. Res.* **12**, 402.
50. Shafi, K.V.P.M.; Gedanken, A.; Goldfarb, R.B.; Felner, I. (1997) *J. Appl. Phys.* **81**, 6901.
51. Suslick, K.S., Grinstaff, M.W. (1990) *J. Am. Chem. Soc.* **112**, 7807.
52. Suslick, K.S.; Grinstaff, M.W. (1992) Proteinaceous Microspheres, *Macromolecular Assemblies*; Stroeve, P.; Balazs, A.C., eds.; Am. Chem. Soc., Washington, D.C.; pp. 218-226.
53. Suslick, K.S.; Grinstaff, M.W.; Kolbeck, K.J.; Wong, M. (1994) *Ultrasonics Sonochem.***1**, S65-S68.
54. Liu, K.J.; Grinstaff, M.W.; Jiang, J.; Suslick, K.S.; Swartz, H.M.; Wang, W. (1994) *Biophys. J.*, **67**, 896-901.
55. Wong, M.; Suslick, K.S. (1995) Sonochemically Produced Hemoglobin Microbubbles, *Hollow and Solid Spheres and Microspheres;* MRS Symp. Proc. v. 372; Wilcox, D.L; Berg, M.; Bernat, T.; Kellerman, D.; Corchran, J.K., eds. Matl. Res. Soc., Pittsburgh, pp 89-94.
56. Eckburg, J.J.; Chato, J.C.; Liu, K.J.; Grinstaff, M.W.; Swartz, H.M.; Suslick, K.S.; Auteri, F. P. (1996), *J. Biomech. Eng. 118*, 193-200.
57. Webb, A.G.; Wong, M.; Kolbeck, K.J.; Magin, R. L.; Wilmes, L. J.; Suslick, K.S. (1996) *J. Mag. Res. Imaging*, **6,** 675-683.
58. Riesz, P.; Berdahl, D.; Christman, C.L. (1985) *Environ. Health Perspect.*, **64**, 233.
59. Keller, M.W.; Feinstein, S.B. in *Echocardiography in Coronary Artery Disease* Kerber, R. E. ed: Future, New York, 1988.
60. Desai, N.P.; Soon-Shiong, P.; Sandford, P.A.; Grinstaff, M.W.; Suslick, K.S. (1994) Magnetic Resonance Imaging with Fluorocarbons Encapsulated in a Cross-linked Polymeric Shell, *U.S. Patent 5,362,478*; Nov. 8, 1994.
61. Desai, N.P.; Soon-Shiong, P.; Sandford, P.A.; Grinstaff, M.W.;Suslick, K.S.; (1995) Methods for *In Vivo* Delivery of Substantially Water Insoluble Pharmacologically Active Agents and Compositions Useful Therefor, *U.S. Patent 5,439,686*; Aug. 8, 1995.
62. Grinstaff, M.W.; Soon-Shiong, P.; Wong, M.; Sandford, P.A.; Suslick, K.S.; Desai, N.P. (1996) Composition Useful for *In Vivo* Delivery of Biologics and Methods Employing Same, *U.S. Patent 5,498,421*; Mar. 12, 1996.
63. Grinstaff, M.W.; Desai, N.P.; Suslick, K.S.; Soon-Shiong, P.; Sandford, P.A.; Merideth, N.R. (1996) Method for the Preparation of Fluorocarbon-Containing Polymeric Shells for Medical Imaging, *U.S. Patent 5,505,932*; Apr. 9, 1996.
64. Grinstaff, M.W.; Desai, N.P.; Suslick, K.S.; Soon-Shiong, P.; Sandford, P.A.; Merideth, N.R. (1996) Non-Fluorinated Polymeric Shells for Medical Imaging, *U.S. Patent 5,508,021*; Apr. 16, 1996.
65. Grinstaff, M.W.; Desai, N.P.; Suslick, K.S.; Soon-Shiong, P.; Sandford, P.A.; Merideth, N.R. (1996) Polymeric Shells for Medical Imaging Prepared from Synthetic Polymers, and Methods for the Use Thereof, *U.S. Patent 5,512,268*; Apr. 30, 1996.
66. Desai, N.P.; Soon-Shiong, P.; Sandford, P.A.; Grinstaff, M.W.;Suslick, K.S. (1996) Methods for *In Vivo* Delivery of Substantially Water Insoluble Pharmacologically Active Agents and Compositions for the Use Thereof *U.S. Patent 5,560,933*; Oct. 1, 1996.
67. Grinstaff, M.W.; Soon-Shiong, P.; Wong, M.; Sandford, P.A.; Suslick, K.S.; Desai, N.P. (1997) Methods for the Preparation of Blood Substitutes for *In Vivo* Delivery, *U.S. Patent 5,635,207*; June 3, 1997.

68. Grinstaff, M.W.; Soon-Shiong, P.; Wong, M.; Sandford, P.A.; Suslick, K.S.; Desai, N.P. (1997) Methods For The Preparation Of Nucleic Acids For In Vivo Delivery, *U.S. Patent 5,639,473;* June 17, 1997.
69. Grinstaff, M.W.; Soon-Shiong, P.; Wong, M.; Sandford, P.A.; Suslick, K.S.; Desai, N.P. (1997) Methods For In Vivo Delivery Of Nutriceuticals And Compositions Useful Therefor, *U.S. Patent 5,650,156;* July 22, 1997.
70. Grinstaff, M.W.; Soon-Shiong, P.; Wong, M.; Sandford, P.A.; Suslick, K.S.; Desai, N.P. (1997) Methods for the Preparation of Pharmaceutically Active Agents for *In Vivo* Delivery, *U.S. Patent 5,665,382*; Sept. 9, 1997.
71. Grinstaff, M.W.; Soon-Shiong, P.; Wong, M.; Sandford, P.A.; Suslick, K.S.; Desai, N.P. (1997) Methods for the Preparation of Immunostimulating Agents for *In Vivo* Delivery, *U.S. Patent 5,665,383*; Sept. 9, 1997.
72. Luche, J.-L. (1996) Comptes Rendus Series IIB **323**, 203 and 337
73. Pestman, J.M., Engberts, J.B.F.N., de Jong, F. (1994) *Recl. Trav. Chim. Pays-Bas*, **113**, 533.
74. Suslick, K.S. (1986) Synthetic Applications of Ultrasound, *Modern Synthetic Methods* **4,** 1-60.
75. Ando, T. Kimura, T. (1991) *Adv. Sonochem.*, **2**, 211.
76. Suslick, K.S., Casadonte, D.J. (1987) *J. Am. Chem. Soc.* **109**, 3459.
77. Suslick, K.S.; Johnson, R.E. (1984) *J. Am. Chem. Soc.* **106**, 6856-6858
78. Suslick, K.S., Doktycz, S.J. (1989) *Chem.Matls.***1**, 6.
79. Suslick, K.S., Doktycz, S.J. (1989) *J. Am. Chem. Soc.* **111**, 2342.
80. Suslick, K.S.; Casadonte, D.J.; Doktycz, S.J. (1989) *Solid State Ionics.* **32/33**, 444-452.
81. Luche, J.-L. (1994) *Ultrasonics Sonochem.*, **1**, S111.
82. Chatakondu, K., Green, M.L.H., Thompson, M.E., Suslick, K.S. (1987) *J. Chem. Soc., Chem. Comm.* **1987**, 900.
83. Suslick, K.S.; Casadonte, D.J.; Green, M.L.H.; Thompson, M.E. (1987) *Ultrasonics* **25**, 56-59
84. Mal'tsev, A.N. (1976) *Zh. Fiz. Khim.* **50**, 1641.